Journal of Power Sources 245 (2014) 27–32

Contents lists available at SciVerse ScienceDirect

Journal of Power Sources

journal homepage: www.elsevier.com/locate/jpowsour

Short communication

Reinvestigation of the electrochemical lithium intercalation in 2H- and 3R-NbS_2

Youhao Liao [a,b], Kyu-Sung Park [b], Preetam Singh [b], Weishan Li [a], John B. Goodenough [b,*]

[a] School of Chemistry and Environment, South China Normal University, Guangzhou 510006, PR China
[b] Texas Materials Institute and Materials Science and Engineering Program, The University of Texas at Austin, Austin, TX 78712, United States

HIGHLIGHTS

- Issues concerning preparation of 2H-NbS_2.
- Cycling of Li into/from 2H-NbS_2 and 3R-NbS_2.
- Influence of pinning of Nb(IV)/Nb(III) couple at top of S–3p bands.

ARTICLE INFO

Article history:
Received 29 March 2013
Received in revised form
6 June 2013
Accepted 7 June 2013
Available online 18 June 2013

Keywords:
2H-niobium disulfide
3R-niobium disulfide
Lithium intercalation
Redox-couple pinning

ABSTRACT

Layered sulfides, 2H-$Li_{0.7}NbS_2$ (s.g.: $P6_3/mmc$) and 3R-NbS_2 (s.g: $R3m$) were synthesized and characterized as electrode materials for a lithium-ion battery. 2H-NbS_2 has been known as a poor electrode material for Li^+-intercalation. However, both 2H-$Li_{0.7}NbS_2$ and 3R-NbS_2 show reversible charge/discharge reactions based on the Nb(IV)/Nb(III) redox couple. They present distinctive differences in the voltage curves as a result of local structural differences. Galvanostatic charge/discharge tests between 1.0 and 3.0 V versus Li showed that discharge capacities were 169.5 mAh g^{-1} for 2H-Li_xNbS_2 and 169.0 mAh g^{-1} for 3R-Li_xNbS_2 at 0.05 C rate and room temperature. At 10 C rate, 2H-Li_xNbS_2 delivered a discharge capacity of 84.0 mAh g^{-1} while 3R-Li_xNbS_2 kept 74.9 mAh g^{-1}. After 200 cycles at 1 C, 9% of capacity fade was observed for 2H-Li_xNbS_2 (from 141.5 to 129.4 mAh g^{-1}) and 3R-Li_xNbS_2 showed 14% fade from 139.4 to 120.1 mAh g^{-1}. The key to improvement of the electrochemical performance of the 2H-Li_xNbS_2 electrode is an initial synthesis of $Li_{0.7}NbS_2$.

1. Introduction

There have been numerous research papers on the intercalation hosts for alkali ions like Li^+ and Na^+ [1,2]. The size difference between the ions often induces an interesting contrast in their electrochemical properties. Recently we have reported the Na-intercalation behavior into 2H-NbS_2, which showed a Na/vacancy ordering at $Na_{0.5}NbS_2$ with stable cycle performance [3]. However, it has been reported that 2H-NbS_2 is not a good Li-intercalation host [4,5], so we revisited the system to find out the origin of the different intercalation behaviors for the 2H- and 3R-NbS_2 structures. As with other layered sulfides, the voltage is restricted to $V < 2.8$ V versus Li^+/Li.

Niobium disulfide, NbS_2, has two known polytype hexagonal structures: one structure with two NbS_2 layers in a unit cell, 2H-NbS_2 (space group: $P6_3/mmc$, No.: 194) and the other with three NbS_2 layers in a unit cell, 3R-NbS_2 (space group: $R3m$, No.: 160) as shown in Fig. 1. In both the 2H and 3R-polytypes, Nb atoms are in trigonal-prismatic sulfur sites and the NbS_3 sites share edges with six nearest NbS_3 neighbors. The NbS_2 slabs are connected weakly by van der Waals forces, and Li can intercalate into the empty octahedral sites of the gallery space in the van der Waals gap. The difference between the two structures is the stacking order of the NbS_6 trigonal prisms, which changes the Li-site environment. In 2H-NbS_2, octahedral-site Li is sandwiched between two NbS_6 prisms along the c-axis while in 3R-NbS_2 Li sits on a site with a NbS_6 prism on one side, an empty prism on the other side.

Layered NbS_2 was first reported by Holleck and Driscoll in 1977 [6] as a cathode to be compared with TiS_2 material for a lithium-ion battery. Later, Kumagai et al. [4] synthesized 2H-NbS_2 at 900 °C and 3R-NbS_2 at 700 °C in a reducing atmosphere for 3 days and investigated the electrochemical performance. It was shown for both 2H- and 3R-NbS_2 that Li_xNbS_2 ($0 < x < 1$) is accessible through an

* Corresponding author. Tel.: +1 512 471 1646; fax: +1 512 471 7681.
E-mail address: jgoodenough@mail.utexas.edu (J.B. Goodenough).

0378-7753/$ – see front matter © 2013 Elsevier B.V. All rights reserved.
http://dx.doi.org/10.1016/j.jpowsour.2013.06.048

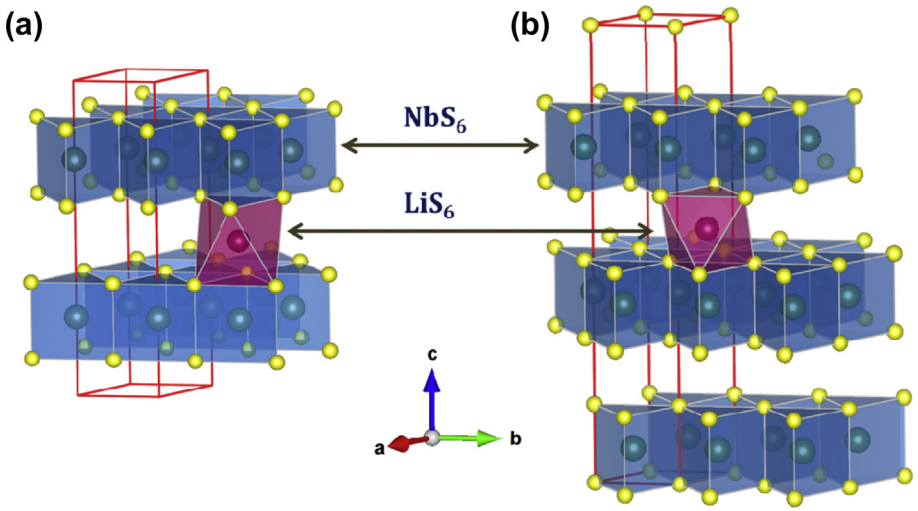

Fig. 1. Crystallographic structures of (a) 2H-NbS_2 and (b) 3R-NbS_2 with LiS_6 octahedral sites (pink in color). (For interpretation of the references to color in this figure legend, the reader is referred to the web version of this article.)

electrochemical charge–discharge process in the voltage range of 1.1–4.1 V in 1 M $LiClO_4$ electrolyte. However, the capacity and cycle performances were quite different: 2H-Li_xNbS_2 showed ~100 mAh g^{-1} at the first discharge and ~75 mAh g^{-1} at the 10th cycle, with the capacity decreasing rapidly after 40 cycles; 3R-Li_xNbS_2 reached ~180 mAh g^{-1} at the first discharge and showed better cycling. After that, Dahn et al. [5] tried to improve the performance of 2H-Li_xNbS_2 by increasing the temperature to 950 °C with 3 days of reaction time to prepare 2H-NbS_2, but unfortunately it still presented a large irreversible capacity loss at the first cycle and didn't show promising cycle performance. Recently, 2H-$Li_{0.63}NbS_2$ and 2H-$Li_{0.7}NbS_2$ were synthesized by separated-reactant metathesis (SRM) to grow single crystals [7,8], which inspired us to consider 2H-Li_xNbS_2 as a starting material to reinvestigate the electrochemical characteristics of 2H-NbS_2 for the electrode of a lithium ion battery. Starting from 2H-$Li_{0.7}NbS_2$, we show that 2H-Li_xNbS_2 can be as good an electrode material as 3R-Li_xNbS_2 for a lithium-ion battery. The reason for the need to start with 2H-$Li_{0.7}NbS_2$ is given in the final paragraph before the conclusion section.

2. Experimental

2H-$Li_{0.7}NbS_2$ was synthesized by solid-state reaction from Li_2S (Alfa Aesar, 99.9% with 5 wt.% excess to compensate for the loss of lithium during calcination), Nb (Alfa Aesar, 99.95%), and S (Alfa Aesar, 99.5%). After mixing the precursor powders, the mixture was pressed into a pellet and put into a carbon-coated quartz tube. The mixing process was done in an argon-filled glove box. The sample tube was evacuated and sealed before calcination. The sample was heated to 700 °C for 20 h and kept at that temperature for 15 h, followed by cooling to 250 °C within 35 h and quenched to room temperature. 3R-NbS_2 with 5 wt.% excess of sulfur was synthesized with the same method except for using an uncoated quartz tube and an annealing condition at 800 °C for 20 h. For comparison, 2H-NbS_2 with 5 wt.% excess of sulfur was also prepared by a solid-state reaction method. A sample pellet in an evacuated uncoated quartz tube was slowly heated to 900 °C and kept at that temperature for 3 days, followed by cooling slowly to 250 °C and finally quenched in air. Preparation of 2H-$LiNbS_2$ by solid state reaction is made difficult by loss of Li, which is why we have prepared 2H-$Li_{0.7}NbS_2$.

X-ray diffraction (XRD) was carried out for phase analyses both of powder and electrode with the PANalytical X'Pert PRO diffractometer with Cu Kα radiation. XRD patterns were collected in the 2-theta range of 10–90° with a step width of 0.02° and a dwell time of 10 s. To avoid any exposure to moisture and oxygen, the XRD sample was put into a sample holder and covered with an amorphous scotch tape in the glove box. The powder morphologies of the prepared samples were checked with a scanning electron microscope (SEM; JEOL, JSM-5610, with an accelerating voltage of 20 kV).

For coin half-cell tests, a composite electrode was fabricated by mixing 75 wt.% of NbS_2 powder (2H-$Li_{0.7}NbS_2$ or 3R-NbS_2), 20 wt.% of acetylene black, and 5 wt.% of polytetrafluoroethylene (PTFE) binder in the glove box. The 2032-type coin cells were assembled with metallic lithium foil as a counter electrode. The electrolyte was 1 M $LiPF_6$ in ethylene carbonate (EC) and diethyl carbonate (DEC) with a volume ratio of 1:1. Cyclic voltammograms (CV) were obtained with a Solartron Analyzer (model 1287) in the potential range of 3.0–1.0 V at a scanning rate of 0.2 mV s^{-1}. Charge/discharge tests were conducted with a Land Battery Test System (Wuhan Land Electronic Co. Ltd).

3. Results and discussion

Fig. 2 exhibits the room-temperature powder X-ray diffraction (XRD) patterns of 2H-$Li_{0.7}NbS_2$ and 3R-NbS_2. The diffraction of 2H-$Li_{0.7}NbS_2$ matches well with the reference diffraction data of hexagonal $Li_{0.7}NbS_2$ (PDF # 04-014-7837; space group: $P6_3/mmc$). The broadened peaks from 15° to 26° are caused by contributions to the signals from the amorphous tape used for sample protection. The 2H-NbS_2 host structure was successfully obtained by adding 0.7 Li per NbS_2, which is also beneficial to the synthetic process by lowering the annealing temperature by 200 °C and shortening the reaction time to 15 h as compared with the previously reported synthetic condition for 2H-NbS_2 (900 °C for 3 days). The presence of Li in NbS_2 enhances the phase stability of the 2H-structure. As shown in Fig. 2, single-phase 3R-NbS_2 was also synthesized; its XRD pattern is well-matched to the standard data of PDF # 04-004-7343. The powder XRD pattern for an as-synthesized 2H-NbS_2 is shown in Fig. 6; it also matches well standard data PDF 04-005-8447.

The powder shape and size of 2H-NbS_2, 2H-$Li_{0.7}NbS_2$, and 3R-NbS_2 were compared and are presented in Fig. 3. In the 2H-

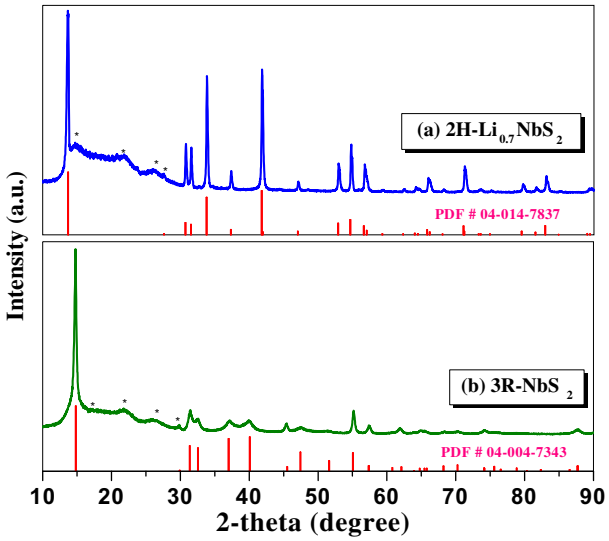

Fig. 2. Powder XRD patterns for (a) 2H-$Li_{0.7}NbS_2$ after annealing at 700 °C for 15 h and (b) 3R-NbS_2 after annealing at 800 °C for 20 h (* denotes the diffraction peaks for scotch tape).

$Li_{0.7}NbS_2$, a bouquet-like texture was observed in secondary particle aggregates composed of sheet-type primary particles with a thickness of around 1 μm. In contrast, large plate-type particles with surface facets were shown for the 2H-NbS_2 structure, Fig. 3(b), which limits their electrochemical properties. The reason for such a great morphology contrast between 2H-NbS_2 and 2H-$Li_{0.7}NbS_2$ is not known. The 3R-NbS_2 also shows secondary particle aggregates, Fig. 3(c), but with thinner primary particles and higher surface area than those of 2H-$Li_{0.7}NbS_2$. In this work, we chose 2H-$Li_{0.7}NbS_2$ instead of 2H-NbS_2 to reveal comparable electrochemical characteristics of 3R-Li_xNbS_2 and 2H-Li_xNbS_2 ($0 < x < 1$).

Fig. 4 presents the cyclic voltammograms of 2H- and 3R-Li_xNbS_2 ($0 < x < 1$) cathodes over the voltage range between 3.0 V and 1.0 V (versus Li^+/Li) with a scanning rate of 0.2 mV s^{-1}. The open-circuit voltage (OCV) for $Li_{0.7}NbS_2$ is as low as ~2.4 V owing to the lithium ions chemically inserted within the van der Waals gaps. A sharp reduction peak at 2.65 V is followed by smaller and broader cathodic peaks at 2.40 V, 2.27 V, and 1.02 V. The oxidation process from Nb(III) to Nb(IV) is almost the same except that the anodic peaks are shifted to 1.04 V, 2.37 V, 2.51 V and 2.80 V, respectively. The current curves of the subsequent cycles (from 2nd to 7th) are almost identical, indicating a highly reversible process of lithiation and delithiation in the 2H-NbS_2 host structure. As is also shown in Fig. 4 for 3R-Li_xNbS_2, four cathodic peaks at 2.44 V, 2.16 V, 1.71 V and 1.11 V can be observed in the reduction process from Nb(IV) to Nb(III). The first reduction behavior is slightly different from that of the following cycles. During oxidation, reversible peaks at 1.22 V, 1.82 V, 2.27 V and 2.55 V are observed. Thus, in both 2H- and 3R-NbS_2, the Li intercalation behavior is rather complicated, but quite reversible.

Similar to the CV data, the galvanostatic charge/discharge tests for 2H- and 3R-NbS_2 also show interesting voltage curves as presented in Fig. 5. The 2H-Li_xNbS_2 profile shows voltage plateaus around 2.75 and 2.7 V followed by a linear curve to 1.9 V. In contrast, 3R-Li_xNbS_2 shows only a sloping voltage curve in the entire voltage range. The higher operating voltage of 2H-Li_xNbS_2 has an advantage as a cathode. The lack of voltage plateaus occurring at voltages where the CV shows peaks may be the result of a slower galvanostatic CV voltage sweep. Changes in Li^+ ordering would take time. Na intercalation in NbS_2 brings distinctive Na/

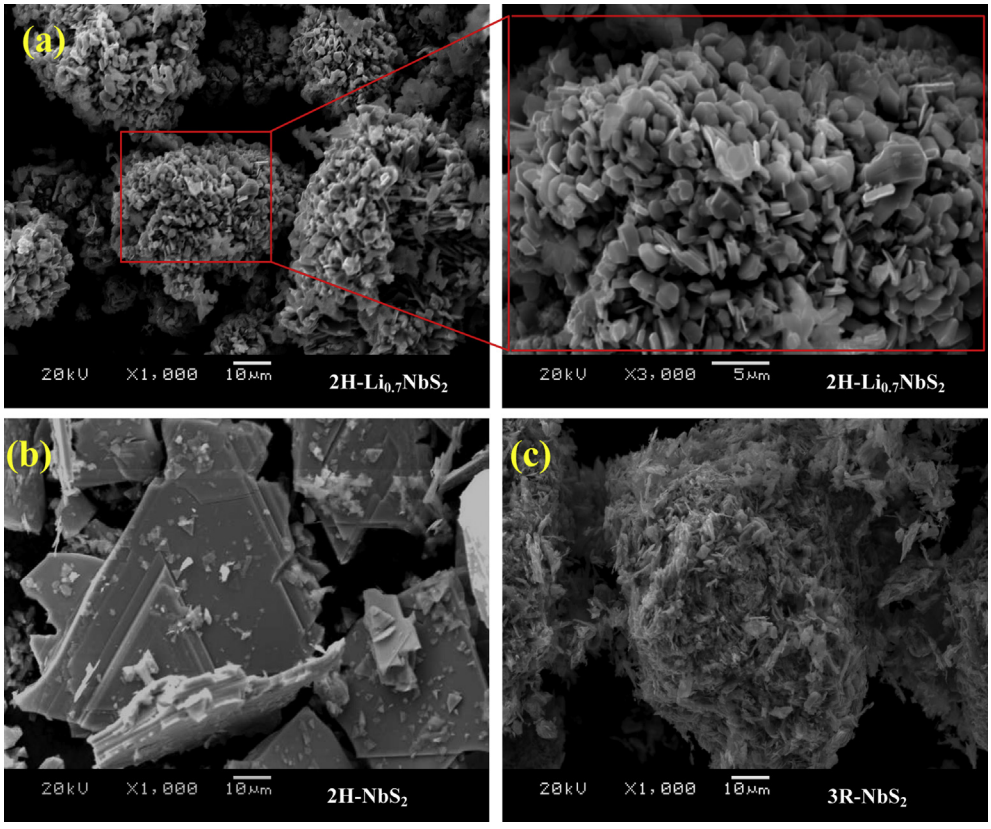

Fig. 3. Powder SEM images of (a) 2H-$Li_{0.7}NbS_2$, (b) 2H-NbS_2 and (c) 3R-NbS_2.

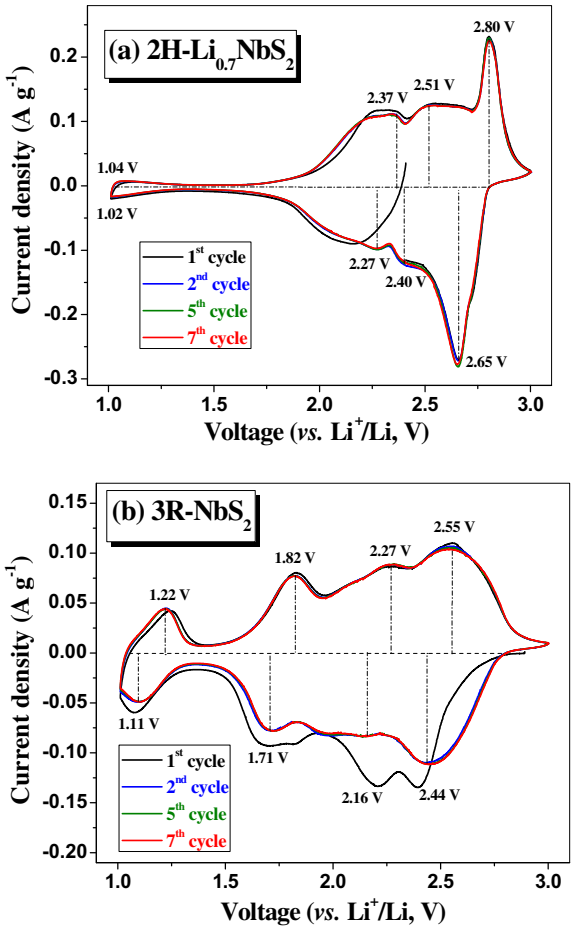

Fig. 4. Cyclic voltammogram of (a) 2H-$Li_{0.7}NbS_2$ and (b) 3R-NbS_2 half cells at over voltage range between 3.0 V and 1.0 V at a scanning rate of 0.2 mV s^{-1}.

vacancy ordering at $Na_{0.5}NbS_2$ [3]. There are similar voltage plateaus at the Na composition $x < 0.4$. In 2H-Na_xNbS_2, DFT calculation shows that forming Na(1)–Na(2) dimers (Na(2) at second or third nearest neighbor sites of Na(1)) is energetically favorable in the dilute limit, which also increases the Na binding energy [3].

Phase changes during charge and discharge were also probed with *ex situ* electrode XRD patterns for Li_0 (charged to 3.0 V) and Li_1 (discharged to 1.0 V) compositions as shown in Fig. 6. The peak position of the 2H-NbS_2 electrode can be matched with the

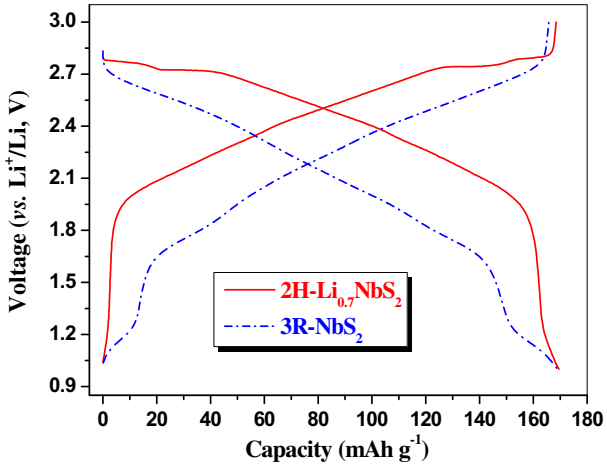

Fig. 5. Charge/discharge voltage curves of 2H-$Li_{0.7}NbS_2$ and 3R-NbS_2 cycled at 0.05 C.

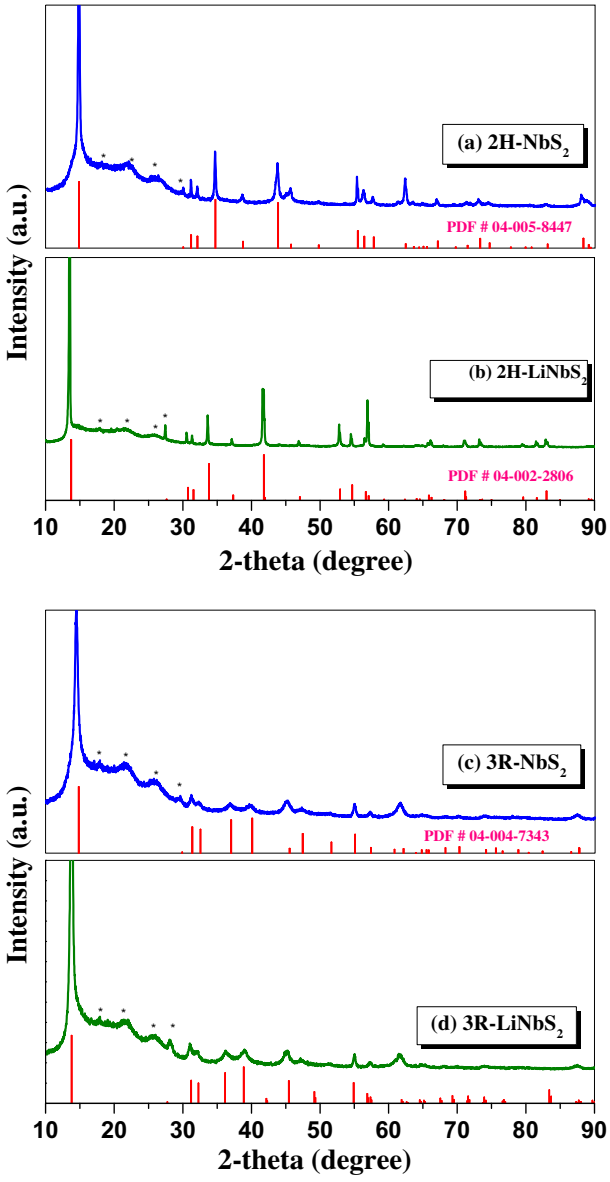

Fig. 6. *Ex situ* electrode XRD patterns of (a) 2H-NbS_2 (charged to 3.0 V), (b) 2H-$LiNbS_2$ (discharged to 1.0 V), (c) 3R-NbS_2 (charged to 3.0 V), and (d) 3R-$LiNbS_2$ (discharged to 1.0 V) (* denotes the diffraction peaks for scotch tape).

standard card (PDF # 04-005-8447, space group: $P6_3/mmc$) except for the relative intensity owing to a preferred orientation of the layered disulfide structure. After discharge to 1.0 V, the XRD pattern of 2H-$LiNbS_2$ agreed well with the standard card of 2H-$LiNbS_2$ (PDF # 04-002-2806, s.g. $P6_3/mmc$). Thus, the 2H-type structure is stable at room temperature at $0 < x < 1$. A similar structural stability is also observed for the 3R-NbS_2 electrodes. After charge, the XRD pattern was matched with the XRD pattern of PDF # 04-004-7343. It is noted that the reference XRD pattern for 3R-$LiNbS_2$ is simulated by the FullProf software with the structure of Fig. 1(b) where the Li atoms are centered at octahedral sites and Nb atoms in trigonal-prismatic sites sharing edges within slabs because no reference data were available. The *ex situ* XRD pattern of 3R-$LiNbS_2$ is consistent with the calculated one, confirming that the space group still remained $R3m$ after Li-intercalation.

The theoretical capacity of NbS_2 for one Li insertion is 170.7 mAh g^{-1}. As shown in Fig. 7(a), the initial discharge capacity of 2H-$Li_{0.7}NbS_2$ is 56.3 mAh g^{-1} ($\approx Li_{0.33}$) at 0.05 C. Thus, considering

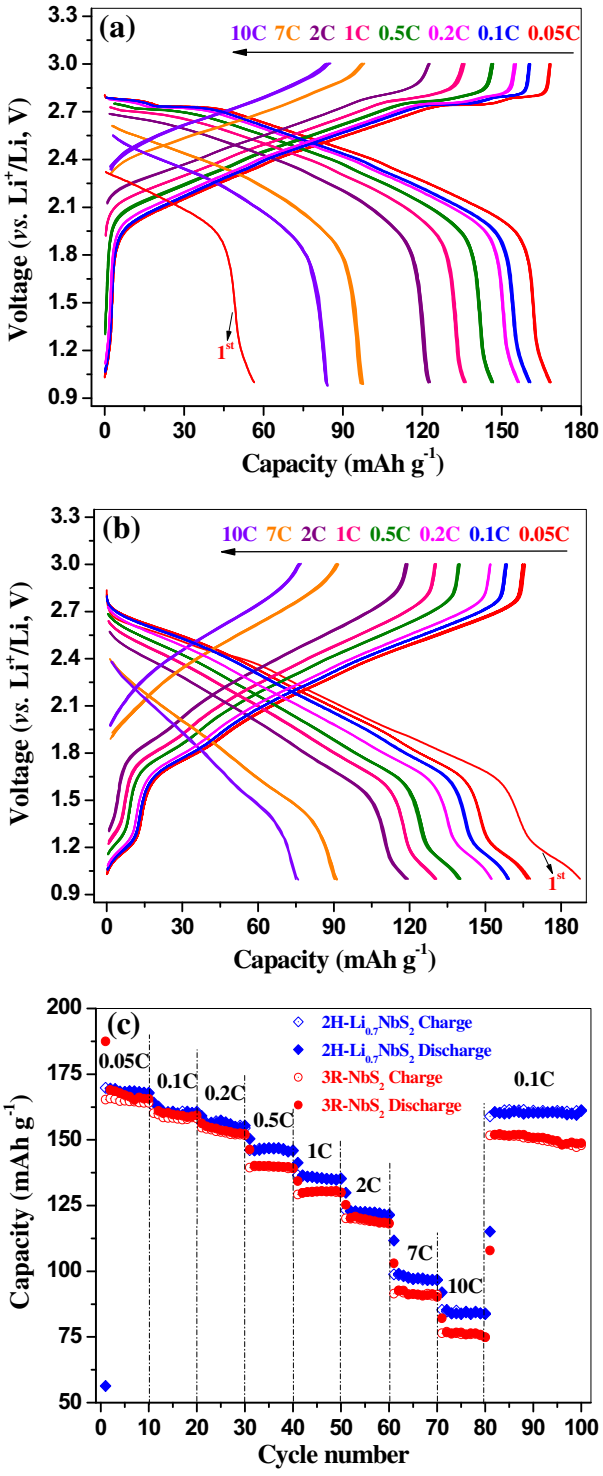

Fig. 7. Representative charge/discharge voltage curves of (a) 2H-$Li_{0.7}NbS_2$, (b) 3R-NbS_2 at different C-rates; and (c) cycle performance at various current densities at room temperature.

possible irreversible electrode/electrolyte reactions, $x \approx 1$ in 2H-Li_xNbS_2 was obtained by discharging the electrode to 1 V. In the following charge process at the 1st cycle, a capacity of 169.8 mAh g^{-1} is observed, which is very close to the theoretical one. Fig. 7(a) also presents the charge and discharge voltage curves of 2H-Li_xNbS_2 at the rates of 0.05 C, 0.1 C, 0.2 C, 0.5 C, 1 C, 2 C, 7 C and 10 C at room temperature; the cycling test is shown in Fig. 7(c). 2H-Li_xNbS_2 prepared by a simple solid-state reaction method shows an impressive rate performance. It shows a discharge capacity of 160.3 mAh g^{-1} at 0.1 C (20th cycle), 135.2 mAh g^{-1} at 1 C (50th cycle), and 84.0 mAh g^{-1} at 10 C (80th cycle). The charge/discharge plateau at around 2.75 V becomes shorter and then disappears with increasing current density. The capacity at 10 C is 49.6% of that at 0.05 C rate, and it was fully recovered to 161.3 mAh g^{-1} when it is retuned to 0.1 C rate (100th cycle). The coulombic efficiency is nearly 100% within 100 cycles. The rate capability is much higher than that of niobium oxides such as $Nb_{12}O_{29}$/C composite and Nb_2O_5 nanobelts [9,10].

The 3R-NbS_2 was also evaluated with the same charge/discharge condition. During the first discharge at 0.05 C rate, as presented in Fig. 7(b), the capacity is 187.5 mAh g^{-1}, which is higher than the theoretical capacity, but it is reduced to 169.0 mAh g^{-1} in the following cycle. The irreversible capacity loss of 22.2 mAh g^{-1} at the first cycle can be related to SEI (solid electrolyte interphase) formation. The loss in 3R-NbS_2 is higher than that of 2H-NbS_2, which can be attributed to the larger surface area as evidenced in Fig. 3. The discharge capacity at 0.1 C rate is 159.3 mAh g^{-1} (20th cycle) and the value becomes 130.0 mAh g^{-1} at 1 C (50th cycle). The capacity is further reduced to 74.9 mAh g^{-1} at 10 C rate (80th cycle) and finally returns to 148.7 mAh g^{-1} at 0.1 C (100th cycle). Formation of the SEI layer can be avoided by cycling to 1.2 V rather than 1.0 V versus Li^+/Li^0.

Fig. 8 exhibits the cycle performance of 2H- and 3R-Li_xNbS_2 electrodes with the charge/discharge rate of 0.05 C for the first 20 cycles and then 1 C for the successive 200 cycles between the voltage range of 1.0 V and 3.0 V. The capacity of 2H-Li_xNbS_2 is a little higher than that of 3R-Li_xNbS_2 and fades less during the 1 C-rate cycles: 9% of the capacity fade for 2H-Li_xNbS_2 (from 141.5 mAh g^{-1} at the 21st to 129.4 mAh g^{-1} at the 220th cycle) and 14% for 3R-Li_xNbS_2 (from 139.4 mAh g^{-1} to 120.1 mAh g^{-1}). Combined with Figs. 7 and 8, the electrochemical performance of 2H-Li_xNbS_2 is improved significantly compared with that of 2H-NbS_2 reported previously; it is even better than that of the 3R-Li_xNbS_2.

It has been known [11] that the top of the S—3p bands in the layered sulfides is at *ca.* 2.7 V versus Li, which means that the Nb(IV)/Nb(III) couple of NbS_2 is pinned at the top of the S—3p bands. The 3R-NbS_2 has the Nb(IV)/Nb(III) couple at a lower voltage ($V < 2.6$ V in Fig. 5), which makes it possible to prepare the 3R phase by solid-state reaction. On the other hand, the higher voltage of the 2H-NbS_2 indicates that attempts to prepare 2H-NbS_2 by solid-state

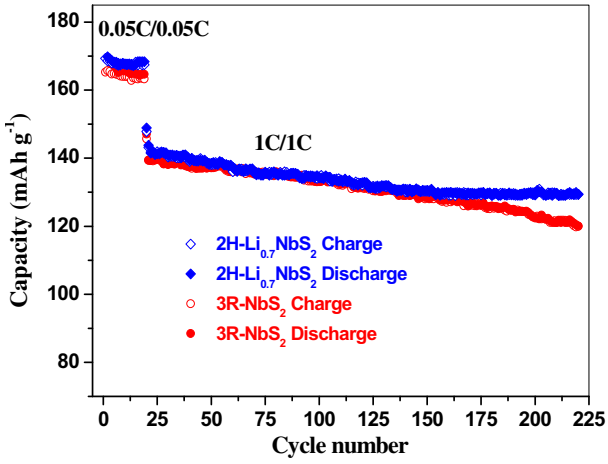

Fig. 8. Cycle performance of 2H-$Li_{0.7}NbS_2$ and 3R-NbS_2 at 0.05 C for the first 20 cycles and 1 C for the successive 200 cycles in the voltage range of 3.0 V and 1.0 V at room temperature.

reaction may encounter oxidation of the sulfur with the formation of disulfide species. By reducing the Nb in $Li_{0.7}NbS_2$, this problem is avoided, and at room temperature access of Nb(IV) is possible; but the short plateau at low x in the charge/discharge curves of 2H-Li_xNbS_2 indicates that at 3 V some reversible formation of disulfide surface species may be occurring. At voltages below *ca.* 1.2 V versus Li, the formation of an SEI layer sets in. Restriction of the voltage range to 1.2 V $\leq x \leq$ 3.0 V should provide excellent cyclability.

4. Conclusion

2H-$Li_{0.7}NbS_2$ and 3R-NbS_2 were synthesized via a solid-state reaction method and characterized as electrode materials for a lithium-ion battery. 2H-NbS_2 has been known as a poor electrode material, but both 2H-$Li_{0.7}NbS_2$ and 3R-NbS_2 showed reversible charge/discharge reactions. The 2H- and 3R-NbS_2 structures have different stacking orders of NbS_2 slabs, which provide octahedral Li-sites with different local environments. The structural difference brings a contrast in the voltage curves. As a result, preparation of the 2H-NbS_2 by solid state reaction is eased by first synthesis of 2H-$Li_{0.7}NbS_2$. Room-temperature cycling tests showed that discharge capacities were 169.5 mAh g^{-1} for 2H-Li_xNbS_2 and 169.0 mAh g^{-1} for 3R-Li_xNbS_2 at 0.05 C rate. 2H-Li_xNbS_2 delivered a discharge capacity of 84.0 mAh g^{-1} while 3R-Li_xNbS_2 kept 74.9 mAh g^{-1} at 10 C. After 200 cycles at 1 C, 9% of capacity fade was observed for 2H-Li_xNbS_2 (from 141.5 to 129.4 mAh g^{-1}) and 3R-Li_xNbS_2 showed 14% fade (from 139.4 to 120.1 mAh g^{-1}). Both 2H- and 3R-structures are good Li^+-intercalation hosts if cycled between 1.0 and 3.0 V, contrary to previous reports.

Acknowledgments

This work was supported by the Robert A Welch Foundation, Grant No. F-1066. Y. Liao thanks the financial support of the joint project of National Natural Science Foundation of China and Natural Science Foundation of Guangdong Province (Grant No. U1134002) and Natural Science Foundation of Guangdong Province (Grant No. 10351063101000001).

References

[1] J.B. Goodenough, K.-S. Park, J. Am. Chem. Soc. 135 (2013) 1167–1176.
[2] V. Palomares, P. Serras, I. Villaluenga, K.B. Hueso, J. Carretero-Gonzalez, T. Rojo, Energy Environ. Sci. 5 (2012) 5884–5901.
[3] Y. Liao, K.-S. Park, P. Xiao, G. Henkelman, W. Li, J.B. Goodenough, Chem. Mater. 25 (2013) 1699–1705.
[4] N. Kumagai, K. Tanno, N. Kumagai, Electrochim. Acta 27 (1982) 1087–1092.
[5] D.C. Dahn, J.F. Carolan, R.R. Haering, Phys. Rev. B 33 (1986) 5214–5220.
[6] G.L. Holleck, J.R. Driscoll, Electrochim. Acta 22 (1977) 647–655.
[7] P.A. Salyer, M.G. Barker, A.J. Blake, D.H. Gregory, C. Wilson, Acta Crystallogr. C59 (2003) i4–i6.
[8] P.A. Salyer, M.G. Barker, D.H. Gregory, M.O. Jones, C. Wilson, Acta Crystallogr. E59 (2003) i112–i115.
[9] Y. Li, C. Sun, J.B. Goodenough, Chem. Mater. 23 (2011) 2292–2294.
[10] M. Wei, K. Wei, M. Ichihara, H. Zhou, Electrochem. Commun. 10 (2008) 980–983.
[11] J.B. Goodenough, Y. Kim, J. Solid State Chem. 42 (2009) 2904–2911.